ACS Photonics

Article

pubs.acs.org/journal/apchd5

Optofluidic Lasers with Monolayer Gain at the Liquid−Liquid Interface

Han Zhang,[†] Anirudh Balram,[‡] Dennis Desheng Meng,[‡] and Yuze Sun*[,†]

[†]Department of Electrical Engineering and [‡]Department of Mechanical Engineering, University of Texas at Arlington, Arlington, Texas 76019, United States

Supporting Information

ABSTRACT: We report optofluidic lasers with a monolayer gain material that self-assembles at the two-phase liquid−liquid interface. The self-assembly process deterministically introduces the gain at the surface of a microdroplet optical cavity, where the lasing mode has maximal interaction with the gain medium. A complete monolayer gain can be achieved in this surface-gain geometry, giving a surface density on the order of 10^{14} cm^{-2}, which proves to be difficult, if not impossible, to achieve in the monolayer gain created at the solid−liquid interface via the surface immobilization method. We demonstrated that the lasing characteristics are drastically different between the gain material that is confined to the liquid−liquid interface and that homogeneously distributed in the bulk liquid solution. Our study reveals the unique capabilities of the surface-gain geometry optofluidic laser, which can be developed into a novel sensing platform to study biophysical and biochemical processes at the molecular level and has vast applications in biomedical diagnostics.

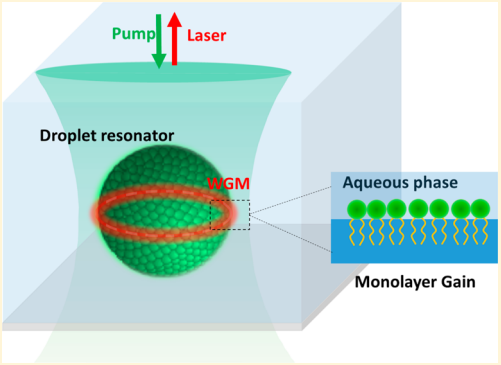

KEYWORDS: *laser, optofluidic laser, self-assembly, surface-gain laser, droplet ring resonator*

Optofluidic lasers, which integrate micro/nanofluidics, optical microcavity, and gain medium in the liquid environment,[1−3] have become an emerging technology in recent years. Compared to gas- and solid-state lasers, the optofluidic laser is unique in its aqueous environment compatibility and adaptive nature of liquids. Therefore, it possesses distinct advantages for applications in bioanalysis and bioimaging[2−7] and for building novel on-chip tunable active photonic devices[8−10] (such as coherent light sources, biocontrolled lasers, light harvesting devices, etc.). In a typical optofluidic laser configuration, the gain material (e.g., organic dyes,[5,8−13] quantum dots,[14,15] fluorescent proteins,[6,16] luciferins[17]) is homogeneously distributed in the entire bulk liquid solution. Although such a gain configuration is simple to implement, the interaction between lasing mode and gain material may not be optimal, which results in poor lasing efficiency and compromised lasing performance. For example, in ring resonators,[5,10,11,16,18,19] certain types of DFBs,[12] and photonic crystals,[20] the lasing modes can interact only with those gain molecules (i.e., a few percent) that are close to the cavity surface through the evanescent field. The rest of the gain molecules in the bulk solution do not participate in lasing, but contribute significantly to an undesirable fluorescence background. To address this problem, a surface-gain geometry optofluidic laser has been studied, where a layer of gain molecules are attached to the surface (e.g., silicon dioxide) of a ring resonator via chemical surface immobilization.[18] Although lasing has been successfully achieved, the intrinsic limitation of a liquid−solid interface makes it challenging, if not impossible, to achieve a complete monolayer of gain at the surface. The surface density of the submonolayer gain materials obtained is strongly dependent on the surface chemistry and immobilization protocols, which are known to cause large variations in molecule surface density and orientation.

Here, we demonstrated an optofluidic microdroplet laser with a monolayer gain material that self-assembles at the two-phase liquid−liquid (oil/water) interface. The self-assembly process deterministically and accurately introduces the gain at the surface of a droplet optical cavity, where the whispering gallery modes (WGMs) have maximal interaction with the gain medium. Compared to the surface immobilization method on a solid substrate, our method does not require time-consuming surface immobilization steps and is highly repeatable in monolayer laser gain formation. Additionally, the surface gain formed at the two-phase liquid−liquid interface offers unprecedented capability to control, modify, program, and engineer the gain medium at the molecular level in an optofluidic laser, thus allowing the laser to be dynamically reconfigured in the most efficient way. In turn, the lasing emission generated in such surface-gain configuration can be conveniently modulated by introducing biological molecules and small chemicals in the aqueous phase to build ultrasensitive

Received: December 9, 2016
Published: February 2, 2017

DOI: 10.1021/acsphotonics.6b00983
ACS Photonics 2017, 4, 621−625

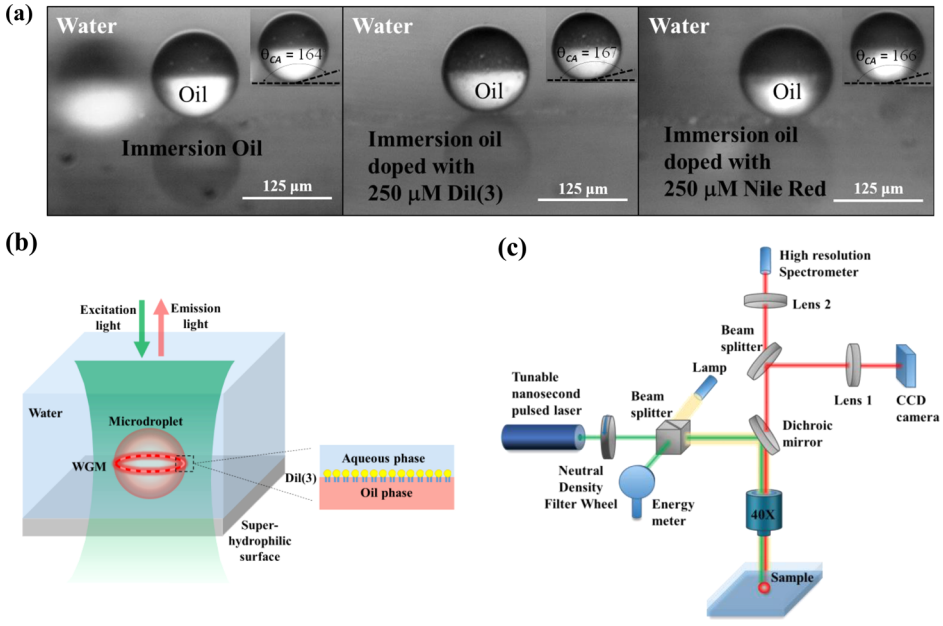

Figure 1. (a) Contact angle characterization of superhydrophilic surface. The contact angle of the oil droplet, Dil(3)-doped oil droplet, and Nile Red-doped oil droplet is 164°, 167°, and 166°, respectively. (b) Schematic illustration of the optofluidic laser with monolayer gain at the liquid–liquid interface. Microdroplets of the oil phase are generated by a microfluidic T-junction and subsequently released into the aqueous phase. A superhydrophilic surface was used to support the microdroplets to allow them to be individually probed by the pump laser. Amphiphilic dye Dil(3) was used as the gain material. WGM: whispering gallery mode. Inset: Illustration of a monolayer of Dil(3) self-assembled at the oil/water interface. (c) Experimental setup for lasing characterization. Microdroplet size was measured by a CCD camera. Lasing emission from the droplet was measured by a spectrometer.

intracavity sensors. Furthermore, a microdroplet naturally serves as a high-Q optical resonator due to its self-organized spherical shape formed by the surface tension and its smooth interface between two-phase fluids (i.e., liquid–air interface or liquid–liquid interface). Therefore, microdroplets are very attractive in the development of ultra-low-threshold lasers.[10,21−23]

In this work, we used a surfactant dye, Dil(3), as the gain material to demonstrate the concept of the surface-gain all-liquid optofluidic laser. When dissolved in oil droplets surrounded by an aqueous phase, Dil(3) diffuses to the droplet surface and self-assembles into a monolayer at the liquid–liquid interface due to its amphiphilic structure (i.e., hydrophilic chromophore and hydrophobic side chains).[24−26] At the right concentration, all gain molecules are located at the oil/water interface, and consequently, there is no free dye in the droplet bulk solution. The WGMs supported by the oil droplets interact with the gain molecules and provide the optical feedback for lasing. We demonstrated lasing from individual oil microdroplets supported by a monolayer of gain at the liquid–liquid interface. To confirm the lasing is indeed from the surface gain, a nonsurfactant dye, Nile Red, is used to generate lasing under otherwise the same experimental conditions. Drastic differences have been observed between the gain material that is confined to the liquid–liquid interface and that homogeneously distributed in the liquid solution.

RESULTS AND DISCUSSION

Dil(3) (1,1′-dioctadecyl-3,3,3′,3′-tetramethylindocarbocyanine perchlorate, Sigma-Aldrich) and Nile Red (Sigma-Aldrich) are dissolved in immersion oil (refractive index = 1.515, Sigma-Aldrich), respectively, to the desired concentration. Dye-doped oil microdroplets are generated using a microfluidic T-junction (see details in the SI). The droplets are subsequently released into a flow cell filled with DI water (refractive index = 1.334). The bottom surface of the flow cell is superhydrophilic, prepared by electrodeposition of nickel cobalt hydroxide with hierarchical micro/nanostructures on a fluorine-doped tin oxide (FTO) glass (see details in the SI). Contact angle measurement on the superhydrophilic surface is presented in Figure 1a, which shows oil droplets and dye-doped oil droplets consistently have a contact angle of above 164°, indicating the superoleophobic nature of the surface under water. The microdroplets on the superhydrophilic surface thus form a nearly perfect spherical resonator with good refractive index contrast to maintain a Q-factor (>10^3). As shown in Figure 1b, the microdroplets can be probed individually by the pump laser light and the lasing emission can be continuously monitored and studied using this technique.

The experimental setup for characterization of lasing emission is illustrated in Figure 1c. The microdroplet was excited with a pulsed optical parametric oscillator laser (repetition rate: 20 Hz, pulse width: 5 ns, wavelength: 532 nm, Continuum). The energy of the pump laser was adjusted with a tunable neutral density filter wheel and monitored by an energy meter (FieldMaxII, Coherent). The pump laser beam was reflected into the flow cell by a dichroic mirror (cutoff wavelength 567 nm, long pass) and focused by a microscope objective (40×, NA = 0.6) to excite the droplets. Through the same objective lens, the emission from the droplet was collected and transmitted through the dichroic mirror and split with a 90/10 beam splitter. One path of the light was collected by a multimode fiber probe and sent to a high-resolution spectrometer (iHR320, Horiba). The other light path went to a CCD camera for imaging and droplet size characterization.

DOI: 10.1021/acsphotonics.6b00983
ACS Photonics 2017, 4, 621−625

To study the lasing capability and performance of the microdroplet laser with a monolayer gain at the liquid−liquid interface, various concentrations (7.5 μM to 1 mM) of Dil(3) oil solutions were used to generate the microdroplets. Those droplets, with a size of 126 ± 11 μm in diameter, were selected for the experiment. An excitation wavelength of 532 nm was used in all experiments. The lasing emission spectra of droplets of different Dil(3) concentrations are shown in Figure 2a,

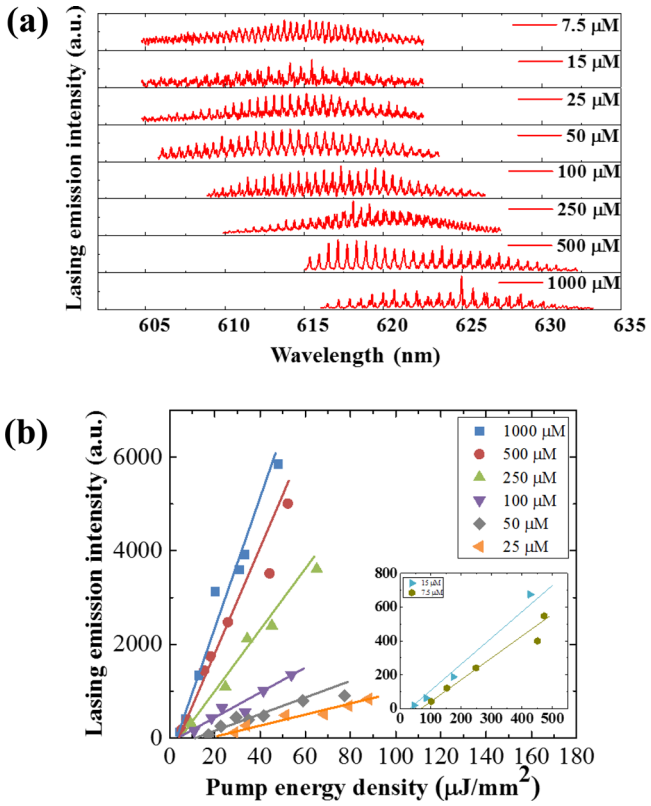

Figure 2. (a) Lasing spectra of microdroplets with different concentrations of Dil(3) (from 7.5 μM to 1 mM), pumped at well above the threshold. Excitation wavelength: 532 nm. (b) Lasing threshold curves. The threshold of a Dil(3) microdroplet is 70 μJ/mm^2 (7.5 μM), 33 μJ/mm^2 (15 μM), 20 μJ/mm^2 (25 μM), 11 μJ/mm^2 (50 μM), 5 μJ/mm^2 (100 μM), 5 μJ/mm^2 (250 μM), 4 μJ/mm^2 (500 μM), and 3 μJ/mm^2 (1 mM), respectively.

which were pumped at well above the threshold. Multiple lasing peaks corresponding to the WGMs with a well-defined free spectral range are clearly observed. The lasing spectrum is centered around 624 nm when the Dil(3) concentration is 1 mM and gradually moves toward the shorter wavelength side of the spectrum when the dye concentration is reduced. The integrated lasing intensity over the entire lasing spectrum (605−632 nm) as a function of the pump energy density is plotted in Figure 2b for each of the dye concentrations shown in Figure 2a.

In order to confirm that the lasing emission in Dil(3) microdroplets is indeed from the monolayer of Dil(3) residing at the oil/water interface, we performed the control experiment using Nile Red as the gain material at otherwise the same experimental conditions. Nile Red is a commonly used gain material in dye lasers. Once dissolved in solution, Nile Red molecules are homogeneously distributed in the microdroplet. In contrast, Dil(3) molecules are preferably diffuse in the oil/water interface and form a monolayer through self-assembly, due to their amphiphilic molecular structure. After Dil(3) molecules saturate the droplet surface, any additional molecules left in the solution will then be homogeneously distributed in the entire volume of the droplet. Due to this key difference in spatial distribution between these two dyes in the microdroplet, the effective gain concentration, as defined by the dye concentration experienced by the WGMs (i.e., total concentration of the dye that interacts with the WGMs), is drastically different for Dil(3) lasers and Nile Red lasers for a given concentration of dye solution used to generate the droplets. To quantitatively compare the effective gain concentration, theoretical calculation is performed for the two dyes respectively and its dependence on the concentration of dye solution used to generate the droplets is shown in Figure 3. For

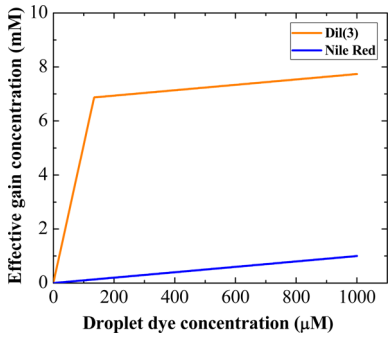

Figure 3. Relation between effective gain concentration and droplet bulk dye concentration for Dil(3) lasers and Nile Red lasers.

the Nile Red microdroplet laser, as well as the majority of other optofluidic dye lasers, the effective gain concentration is equal to the dye solution concentration used to generate the droplets (i.e., bulk solution concentration in the droplet). However, for the Dil(3) microdroplet laser the effective gain concentration is much higher than the dye solution concentration used to generate the droplets because dye molecules are favorably accumulated at the surface. The turning point in the Dil(3) curve shown in Figure 3 occurs at the critical concentration, where the number of Dil(3) molecules in the bulk solution is just enough to form a monolayer gain at the droplet surface and there are no free dye molecules left in the solution. The details on the analysis of the surface accumulation effect on gain molecules and the effective gain concentration calculation are documented in the SI. Since effective gain concentration is equivalent to the number of dye molecules that are capable of participating in lasing, the surface-gain geometry laser is intrinsically more efficient and advantageous compared to conventional optofluidic dye lasers.

Lasing emission spectra and threshold curves for different dye concentrations are measured for the Nile Red microdroplet laser, as shown in Figure S2 (see details in the SI). To compare the surface-gain and bulk-gain configuration in optofluidic lasers, lasing threshold values of Dil(3) and Nile Red lasers at different droplet dye concentrations are plotted in Figure 4a. When the dye concentration is reduced, the Nile Red lasing threshold increases almost linearly on a logarithmic scale. However, due to the surface accumulation effect, the lasing threshold stays almost unchanged when the concentration is above the critical concentration, where a complete monolayer gain is formed at the droplet interface. When the dye concentration is below the critical concentration, a submono-

DOI: 10.1021/acsphotonics.6b00983
ACS Photonics 2017, 4, 621−625

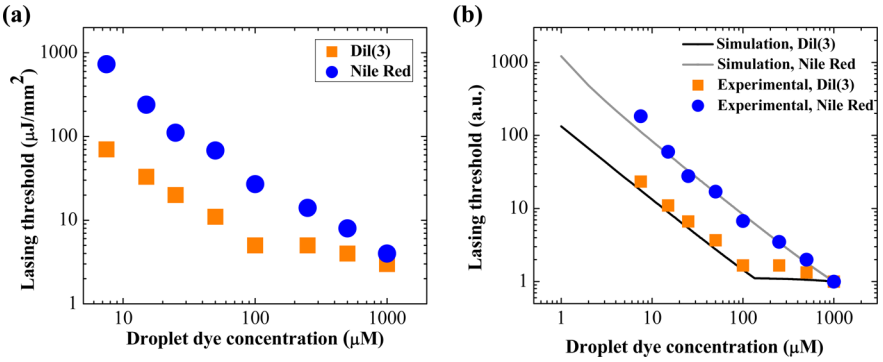

Figure 4. Lasing threshold for Dil(3) and Nile Red microdroplets and their dependence on the microdroplet dye concentration. (a) Experimental results. (b) Simulation results of normalized lasing threshold. Droplet cavity *Q*-factor of 5×10^3 is used in the simulation.

layer of gain material is located at the droplet interface. Lasing can still be sustained in this region. However, the lasing threshold increases quickly with decreased dye concentration, similar to that observed in bulk-geometry optofluidic lasers.

To further understand the lasing characteristics between surface-gain and bulk-gain configuration in optofluidic lasers, a theoretical analysis is performed on two types of lasers (see details in the SI). The lasing threshold, I_{th}, is determined by[5,18]

$$I_{th} = \frac{\gamma}{1-\gamma} \tag{1}$$

where γ is the fraction of gain molecules in the excited state at the threshold.

$$\gamma = \frac{\sigma_a(\lambda_L)}{\sigma_e(\lambda_L) + \sigma_a(\lambda_L)}\left[1 + \frac{Q_{abs}}{Q_0}\right] \tag{2}$$

where $\sigma_e(\lambda_L)$ ($\sigma_a(\lambda_L)$) is the dye emission cross-section (dye absorption cross-section) at the lasing wavelength λ_L, Q_0 is the microdroplet empty-cavity quality factor, and $Q_{abs} = 2\pi m/\lambda_L n_t \sigma_a(\lambda_L)$ is the quality factor related to the dye absorption. n_T is the total concentration of the dye. m is the effective refractive index of the WGMs ($m \approx 1.515$). The dye emission cross-section and absorption cross-section are measured experimentally. Using experimentally measured data (see details in the SI), we calculate the Dil(3) emission cross-section at a lasing wavelength of $\lambda_{L,Dil(3)} = 618$ nm to be $\sigma_e(\lambda_{L,Dil(3)}) = 7.98 \times 10^{-17}$ cm^2 and the Nile Red emission cross-section at a lasing wavelength of $\lambda_{L,Nile\ Red} = 635$ nm to be $\sigma_e(\lambda_{L,Nile\ Red}) = 1.46 \times 10^{-16}$ cm^2. The absorption cross-section of Dil(3) and Nile Red in the lasing wavelength region are extrapolated from their respective absorption spectrum, from which $\sigma_a(\lambda_{L,Dil(3)}) = 1 \times 10^{-21}$ cm^2 and $\sigma_a(\lambda_{L,Nile\ Red}) = 1.2 \times 10^{-20}$ cm^2 are obtained. Since direct measurement of the empty-cavity quality factor Q_0 is challenging in microdroplets, Q_0 values in the range of 10^3 to 10^5 are scanned in the simulation, and the results on the threshold dependence on droplet dye bulk concentration for Dil(3) and Nile Red are compared to the experimental results to determine the empty-cavity *Q*-factor of our droplet lasers. From the results shown in Figure 4b, Q_0 is estimated to be around 5×10^3.

It is worth noting that there is a unique turning point in the lasing threshold–concentration curve, as demonstrated in Figure 4, in the surface-gain type of the optofluidic laser formed at the two-phase liquid–liquid interface. This turning point corresponds to the critical concentration discussed previously, where a complete monolayer is self-assembled at the interface, which in turn is determined by the packing geometry (i.e., molecular spacing) of the gain molecules. Therefore, by mapping out the turning point in the threshold–concentration curve, the optofluidic laser platform demonstrated here could provide a convenient method to characterize molecular spacing. By linear fitting of the measurement data in the region below and above the critical concentration in Figure 4a, the critical concentration is estimated to be 122 μM, which yields a molecular spacing of 8 Å. This number is comparable to the molecular spacing of phospholipid molecules in liposome and lipid bilayer structures reported in other works.[27,28]

In summary, we have developed an optofluidic droplet laser with surface gain precisely located at the two-phase liquid–liquid interface. Lasing emission from monolayer gain and submonolayer gain have been achieved. The unique surface-gain geometry enables all gain material to participate in lasing and thus greatly increases laser efficiency compared to the conventional optofluidic laser, where gain material is homogeneously distributed in the entire laser cavity. We have further demonstrated that the lasing threshold in a surface-gain type of optofluidic laser is very sensitive to the molecular spacing and packing geometry at the interface. Our technology could be potentially useful in studying phospholipids' surface density and molecular orientation and small-molecule interaction dynamics with the cell membrane, all of which currently require the use of advanced technologies such as NMR, atomic force microscopy, and fluorescence microscopy.

■ ASSOCIATED CONTENT

Supporting Information

The Supporting Information is available free of charge on the ACS Publications website at DOI: 10.1021/acsphotonics.6b00983.

Superhydrophilic surface fabrication, droplet generation, lasing performance of Nile Red microdroplet laser, theoretical analysis of microdroplet dye laser, fluorescence lifetime measurement, absorption cross-section measurement, and quantum yield measurement (PDF)

■ AUTHOR INFORMATION

Corresponding Author

*E-mail: sun@uta.edu.

ORCID

Yuze Sun: 0000-0001-5149-2277

Notes

The authors declare no competing financial interest.

DOI: 10.1021/acsphotonics.6b00983
ACS Photonics 2017, 4, 621–625

■ ACKNOWLEDGMENTS

The authors are grateful for the support from the National Science Foundation (Grant Nos. 1554013, 1439494, and 1444473) and the ORAU Ralph E. Powe Junior Faculty Enhancement Award.

■ REFERENCES

(1) Li, Z.; Psaltis, D. Optofluidic dye lasers. *Microfluid. Nanofluid.* **2008**, *4*, 145−158.
(2) Fan, X.; White, I. M. Optofluidic microsystems for chemical and biological analysis. *Nat. Photonics* **2011**, *5*, 591−597.
(3) Fan, X.; Yun, S.-H. The potential of optofluidic biolasers. *Nat. Methods* **2014**, *11*, 141−147.
(4) Chen, Y.; Lei, L.; Zhang, K.; Shi, J.; Wang, L.; Li, H.; Zhang, X. M.; Wang, Y.; Chan, H. L. W. Optofluidic microcavities: Dye-lasers and biosensors. *Biomicrofluidics* **2010**, *4*, 043002.
(5) Sun, Y.; Fan, X. Distinguishing DNA by Analog-to-Digital-like Conversion by Using Optofluidic Lasers. *Angew. Chem., Int. Ed.* **2012**, *51*, 1236−1239.
(6) Gather, M. C.; Yun, S. H. Single-cell biological lasers. *Nat. Photonics* **2011**, *5*, 406−410.
(7) Wu, X.; Oo, M. K. K.; Reddy, K.; Chen, Q.; Sun, Y.; Fan, X. Optofluidic laser for dual-mode sensitive biomolecular detection with a large dynamic range. *Nat. Commun.* **2014**, *5*, 3779.
(8) Helbo, B.; Kristensen, A.; Menon, A. A micro-cavity fluidic dye laser. *J. Micromech. Microeng.* **2003**, *13*, 307.
(9) Li, Z.; Zhang, Z.; Emery, T.; Scherer, A.; Psaltis, D. Single mode optofluidic distributed feedback dye laser. *Opt. Express* **2006**, *14*, 696−701.
(10) Tang, S. K.; Li, Z.; Abate, A. R.; Agresti, J. J.; Weitz, D. A.; Psaltis, D.; Whitesides, G. M. A multi-color fast-switching microfluidic droplet dye laser. *Lab Chip* **2009**, *9*, 2767−2771.
(11) Chen, Q.; Liu, H.; Lee, W.; Sun, Y.; Zhu, D.; Pei, H.; Fan, C.; Fan, X. Self-assembled DNA tetrahedral optofluidic lasers with precise and tunable gain control. *Lab Chip* **2013**, *13*, 3351−3354.
(12) Song, W.; Vasdekis, A. E.; Li, Z.; Psaltis, D. Optofluidic evanescent dye laser based on a distributed feedback circular grating. *Appl. Phys. Lett.* **2009**, *94*, 161110.
(13) Azzouz, H.; Alkhafadiji, L.; Balslev, S.; Johansson, J.; Mortensen, N. A.; Nilsson, S.; Kristensen, A. Levitated droplet dye laser. *Opt. Express* **2006**, *14*, 4374−4379.
(14) Kiraz, A.; Chen, Q.; Fan, X. Optofluidic Lasers with Aqueous Quantum Dots. *ACS Photonics* **2015**, *2*, 707−713.
(15) Schäfer, J.; Mondia, J. P.; Sharma, R.; Lu, Z. H.; Susha, A. S.; Rogach, A. L.; Wang, L. J. Quantum dot microdrop laser. *Nano Lett.* **2008**, *8*, 1709−1712.
(16) Chen, Q.; Zhang, X.; Sun, Y.; Ritt, M.; Sivaramakrishnan, S.; Fan, X. Highly sensitive fluorescent protein FRET detection using optofluidic lasers. *Lab Chip* **2013**, *13*, 2679−2681.
(17) Wu, X.; Chen, Q.; Sun, Y.; Fan, X. Bio-inspired optofluidic lasers with luciferin. *Appl. Phys. Lett.* **2013**, *102*, 203706.
(18) Chen, Q.; Ritt, M.; Sivaramakrishnan, S.; Sun, Y.; Fan, X. Optofluidic lasers with a single molecular layer of gain. *Lab Chip* **2014**, *14*, 4590−4595.
(19) Sun, Y.; Shopova, S. I.; Wu, C.-S.; Arnold, S.; Fan, X. Bioinspired optofluidic FRET lasers via DNA scaffolds. *Proc. Natl. Acad. Sci. U. S. A.* **2010**, *107*, 16039−16042.
(20) Zhen, B.; Chua, S.-L.; Lee, J.; Rodriguez, A. W.; Liang, X.; Johnson, S. G.; Joannopoulos, J. D.; Soljačić, M.; Shapira, O. Enabling enhanced emission and low-threshold lasing of organic molecules using special Fano resonances of macroscopic photonic crystals. *Proc. Natl. Acad. Sci. U. S. A.* **2013**, *110*, 13711−13716.
(21) Qian, S.-X.; Snow, J. B.; Tzeng, H.-M.; Chang, R. K. Lasing droplets: highlighting the liquid-air interface by laser emission. *Science* **1986**, *231*, 486−488.
(22) Kiraz, A.; Sennaroglu, A.; Doğanay, S.; Dündar, M.; Kurt, A.; Kalaycıoğlu, H.; Demirel, A. Lasing from single, stationary, dye-doped glycerol/water microdroplets located on a superhydrophobic surface. *Opt. Commun.* **2007**, *276*, 145−148.
(23) Humar, M.; Yun, S. H. Intracellular microlasers. *Nat. Photonics* **2015**, *9*, 572.
(24) Holler, S.; Goddard, N. L.; Arnold, S. Spontaneous emission spectra from microdroplets. *J. Chem. Phys.* **1998**, *108*, 6545−6547.
(25) Folan, L.; Arnold, S. Determination of molecular orientation at the surface of an aerosol particle by morphology-dependent photoselection. *Opt. Lett.* **1988**, *13*, 1−3.
(26) Aas, M.; Jonáš, A.; Kiraz, A. Lasing in optically manipulated, dye-doped emulsion microdroplets. *Opt. Commun.* **2013**, *290*, 183−187.
(27) Ruaudel-Teixier, A.; Vandevyver, M. Energy transfer in dye monomolecular layers. *Thin Solid Films* **1980**, *68*, 129−133.
(28) Huang, C.-H.; Mason, J. Geometric packing constraints in egg phosphatidylcholine vesicles. *Proc. Natl. Acad. Sci. U. S. A.* **1978**, *75*, 308−310.

DOI: 10.1021/acsphotonics.6b00983
ACS Photonics 2017, 4, 621−625